Nonlinear Adaptive Observer for a Lithium-Ion Battery Cell Based on Coupled Electrochemical–Thermal Model

S. Dey[1]
Department of Automotive Engineering,
Clemson University,
4 Research Drive,
Greenville, SC 29607
e-mail: satadrd@clemson.edu

B. Ayalew
Department of Automotive Engineering,
Clemson University,
4 Research Drive,
Greenville, SC 29607
e-mail: beshah@clemson.edu

P. Pisu
Department of Automotive Engineering,
Clemson University,
4 Research Drive,
Greenville, SC 29607
e-mail: pisup@clemson.edu

Real-time estimation of battery internal states and physical parameters is of the utmost importance for intelligent battery management systems (BMS). Electrochemical models, derived from the principles of electrochemistry, are arguably more accurate in capturing the physical mechanism of the battery cells than their counterpart data-driven or equivalent circuit models (ECM). Moreover, the electrochemical phenomena inside the battery cells are coupled with the thermal dynamics of the cells. Therefore, consideration of the coupling between electrochemical and thermal dynamics inside the battery cell can be potentially advantageous for improving the accuracy of the estimation. In this paper, a nonlinear adaptive observer scheme is developed based on a coupled electrochemical–thermal model of a Li-ion battery cell. The proposed adaptive observer scheme estimates the distributed Li-ion concentration and temperature states inside the electrode, and some of the electrochemical model parameters, simultaneously. These states and parameters determine the state of charge (SOC) and state of health (SOH) of the battery cell. The adaptive scheme is split into two separate but coupled observers, which simplifies the design and gain tuning procedures. The design relies on a Lyapunov's stability analysis of the observers, which guarantees the convergence of the combined state-parameter estimates. To validate the effectiveness of the scheme, both simulation and experimental studies are performed. The results show that the adaptive scheme is able to estimate the desired variables with reasonable accuracy. Finally, some scenarios are described where the performance of the scheme degrades.
[DOI: 10.1115/1.4030972]

Introduction

Li-ion batteries are now the leading solutions for electrified transportation and stationary energy storage applications due to their several beneficial features in high energy and power density, absence of memory effect and self-discharge, low environmental impact, etc. However, they still suffer from safety and reliability concerns. These concerns can be addressed via the advanced BMS, which require precise knowledge of battery internal information like SOC and SOH.

The core challenge for acquiring these internal information is that, in general, the only available information in real-time is boundary measurement of voltage, current, and temperature. This fact underscores the importance of reliable estimation algorithms that compute the internal information in the Li-ion cells from these limited measurements. Moreover, there are several other challenges in SOC and SOH estimation of Li-ion cells [1]. One of them arises from the spatially distributed nature of Li-ion concentrations inside the cell. Other crucial challenges relate to parametric uncertainties with aging (both with charge/discharge history and calendar time), cell-to-cell manufacturing variability, and variations in Li-ion chemistry. In this paper, we address some of these challenges by proposing an electrochemical–thermal model-based adaptive estimation scheme for online joint estimation of the distributed Li-ion concentration in the electrodes, and some uncertain model parameters. In addition to improving the accuracy of the SOC estimation, online parameter estimates can be used as SOH indicators.

In the literature, the different estimation algorithms proposed for Li-ion batteries can be broadly classified based on the type of model used: (1) data-driven model-based algorithms [2,3], (2) ECM-based algorithms [4–7], and (3) electrochemical model-based algorithms. Although data-driven approaches are simple in implementation and design, the drawback lies in the requirement of large amount of data over the whole operating regime of the battery and lack of physical meaning of the data-driven model parameters. Similarly, the parameters of the ECM based approaches (for example, the resistors and capacitors) have to be modeled as functions of different operating conditions such as SOC, temperature, etc., to capture the battery behavior over larger operating range.

Electrochemical model-based approaches, developed from porous electrode and concentrated solution theories, are more accurate compared to other kinds of models [8]. However, full-order electrochemical model (pseudo-two-dimensional (P2D) model) consists of coupled nonlinear partial differential equations (PDE) [9]. A few methods exist in literature that improves the computational efficiency of P2D model, for instance in Ref. [10], a Legendre polynomial and Galerkin projection based approach is used. However, the complex mathematical structure of P2D model still remains one of the difficult factors for suitable estimator design. This complex mathematical structure has led to different kinds of model reductions in the literature before the estimator is designed. For example, a residue grouping with a linear Kalman filter was used in Ref. [11] and a constant electrolyte concentration assumption with Luenberger observer was used in Ref. [12]. In Ref. [13], a reduced-order electrochemical model is developed using quasi-linearization and Pade approximation. Recently, a physics-based second-order Li-ion battery model is presented in Ref. [14]. Another reduced-order electrochemical model called the single particle model (SPM) where the electrodes are

[1]Corresponding author.

Contributed by the Dynamic Systems Division of ASME for publication in the Journal of Dynamic Systems, Measurement, and Control. Manuscript received December 17, 2014; final manuscript received June 18, 2015; published online August 13, 2015. Assoc. Editor: Junmin Wang.

approximated as spherical particles is also popular in SOC estimator designs [15–17]. The authors of the present paper proposed SPM-based nonlinear observer designs for the SOC estimation in Refs. [18,19].

Unlike the well-investigated SOC estimation problem, adaptive SOC estimation or the simultaneous state-parameter estimation problem is relatively less explored for electrochemical models. Some of the existing works use multirate particle filter [20], unscented Kalman filter [21], iterated extended Kalman filter [22,23] for adaptive SOC estimation. The drawback of these approaches lies in the difficulty to theoretically verify the convergence of the estimators. In another work [24], an adaptive PDE observer and least square parameter estimator based framework is presented for the same problem. However, stability of the combined state and parameter estimators was not verified analytically. In Refs. [25,26], a nonlinear geometric observer based approach is presented for adaptive estimation of battery SOC and parameters with theoretical verification of error convergence. However, the Li-ion diffusion dynamics and the Li-ion spatial distribution in the battery electrode are ignored. Moreover, thermal effects are not considered. As will be seen later, the approach presented in present paper takes the Li-ion diffusion and spatial distribution into consideration along with considering the thermal effects. The authors of the current paper also proposed a sliding mode observer based approach in Ref. [27] for adaptive estimation of SOC. However, the drawback of the approach is that a high initial error in contact resistance estimation may lead to instability of the scheme. Other than adaptive estimation techniques, recently a SOH monitoring technique is presented that essentially monitors the side reaction current density of the battery via retrospective cost-subsystem identification [28,29].

Other than SOC and SOH, battery temperature is another important quantity that is used by BMS for thermal management of the batteries. Some recent results exist in literature for temperature estimation. For example, a linear parameter varying observer-based approach is presented in Ref. [30] for temperature estimation of automotive battery packs. A lumped parameter thermal model has been presented in Ref. [31] to capture surface and core temperature of the battery and used for adaptive observer-based temperature estimation along with health monitoring via internal resistance estimation [32]. Further, the work [32] is extended to temperature estimation under unknown cooling condition [33] and to parameterization and observability analysis of a battery cluster [34]. However, these approaches use ECM to capture the battery electrical and SOC dynamics. In Ref. [35], an enhanced SPM is used considering temperature and electrolyte effects to design a Luenberger observer for SOC estimation. However, the model parameters were assumed to be known and parameter estimation problem is not addressed. In this paper, we extend these researches by presenting an electrochemical model-based state-parameter estimation approach considering the thermal dynamics of the battery cell.

From the above review, it can be noted that most of the electrochemical–model based adaptive estimation approaches cited above consider only electrochemical dynamics under isothermal conditions. However, there is a bidirectional coupling between the electrochemical and thermal dynamics of a Li-ion cell. In Refs. [12,36], numerical and experimental results have shown that inclusion of the thermal model may lead to significant improvement in the SOC estimation accuracy. This observation is also consistent with the physical behavior of the cell which shows a bidirectional coupling captured by the coupled model as follows: in electrochemical model, the open circuit potential and some parameters are affected by temperature changes, whereas in the thermal model, the electrochemical overpotential and open circuit potential contribute to heat generation [37].

To address the above issues, we proposed a Lyapunov-based nonlinear adaptive observer design based on a combined electrochemical–thermal model of a Li-ion cell in Ref. [38]. In this paper, we extend this preliminary work by including the following: (1) detailing the discussion on the modeling of the Li-ion cell, (2) relaxing the constant contact resistance assumption of our previous work [38] and re-establishing the convergence proof of the adaptive observer considering temperature dependence of the contact resistance, (3) adding experimental studies on a commercial Li-ion cell, and (4) including discussions on the limitations of the proposed observer scheme. We also provide an analytical proof of convergence for the overall adaptive scheme combining state and parameter estimators. In this study, we utilize the single particle electrochemical model (SPM) along with lumped thermal dynamics [39] to derive the adaptive observers. Three parameters, namely, diffusion coefficient, contact resistance, and active material volume fraction, are estimated along with the SOC, and may be used as SOH indicators [40].

The rest of the paper is organized as follows: The section, Lithium-Ion Cell Electrochemical-Thermal Model, discusses the electrochemical–thermal modeling of Li-ion cell. After that the adaptive scheme is described. Next, simulation and experimental results are provided. Then some potential failure scenarios are illustrated for the adaptive scheme, and finally, the concluding remarks are summarized.

Lithium-Ion Cell Electrochemical–Thermal Model

The benchmark Li-ion cell electrochemical model is the P2D model derived from the porous electrode and concentrated solution theories [9]. It describes mass and charge conservation in the solid active material and the electrolyte along with the electrochemical kinetics described by Butler–Volmer equation. Although there exist some approaches, e.g., [10] that improve the computational efficiency of P2D model, the complex mathematical structure still makes it unsuitable for real-time estimator design. Owing to this, researchers generally resort to model reduction techniques to derive a model suitable for real-time estimator design. The SPM is one of the popular reduced electrochemical models that we adopt in this paper.

Essentially, the SPM is derived by approximating each electrode as a single spherical particle and applying volume-averaging assumptions [15,16]. This approximation leads to two linear diffusion PDEs for Li-ion mass conservation in both electrodes given by Eq. (1). The output voltage map is derived from Butler–Volmer kinetics, electrical potential, and electrode thermodynamics and is given by Eq. (2)

$$\frac{\partial c_s^{\pm}}{\partial t} = \frac{D_s^{\pm}(T)}{r^2}\frac{\partial}{\partial r}\left(r^2\frac{\partial c_s^{\pm}}{\partial r}\right)$$
$$\left.\frac{\partial c_s^{\pm}}{\partial r}\right|_{r=0} = 0, \quad \left.\frac{\partial c_s^{\pm}}{\partial r}\right|_{r=R} = \frac{\pm I}{a_s^{\pm}FD_s^{\pm}(T)AL^{\pm}} \tag{1}$$

$$V = \frac{\bar{R}T}{\bar{\alpha}^{+}F}\sinh^{-1}\left(\frac{I}{2a_s^{+}AL^{+}i_0^{+}}\right) - \frac{\bar{R}T}{\bar{\alpha}^{-}F}\sinh^{-1}\left(\frac{I}{2a_s^{-}AL^{-}i_0^{-}}\right) + U^{+}\left(c_{s,e}^{+},T\right) - U^{-}\left(c_{s,e}^{-},T\right) - R_f(T)I \tag{2}$$

where U^{+} and U^{-} are the open-circuit potentials as functions of Li-ion surface concentration and temperature, $c_s^{\pm}$ is the Li-ion concentration of the positive and negative electrode, $c_{s,e}^{+}$ and $c_{s,e}^{-}$ are the surface concentrations of the positive and negative electrode, V is the output voltage, and I is the input current (the reader may refer to the Nomenclature for the definitions of the rest of the variables). The $i_0^{\pm}$ are the exchange current densities given by

$$i_0^{\pm} = K^{\pm}(T)\sqrt{c_e c_{s,e}^{\pm}\left(c_{s,\max}^{\pm} - c_{s,e}^{\pm}\right)} \tag{3}$$

Along with the electrochemical SPM model, the following lumped thermal model derived from the energy balance of the cell is considered [39] and is given by

$$\rho v C_p \frac{dT}{dt} = I\left(U^+\left(c^+_{s,e},T\right) - U^-\left(c^-_{s,e},T\right) - V - T\left(\frac{\partial U^+}{\partial T} - \frac{\partial U^-}{\partial T}\right)\right) - hA_s(T - T_\infty) \tag{4}$$

where T is the lumped averaged temperature of the cell and $(\partial U^{\pm}/\partial T)$ are functions of $c^{\pm}_{s,e}$ [39]. Here, a thermal modeling approach in Refs. [39,41] is followed where a lumped thermal model is applied that predicts a lumped-temperature averaged over the cell. However, more detailed thermal model, e.g., the one in Refs. [31,32] can be applied here which may be considered as a future extension of the present work. Now considering (4), note that the temperature affects the open-circuit potential and over potential terms in Eq. (2), whereas $U^{\pm}$ and $\partial U^{\pm}/\partial T$ contribute to the heat generation in Eq. (4). Moreover, in this study, we assume that the solid phase diffusion coefficients ($D^{\pm}_s$) and the reaction rate constants ($K^{\pm}$) show Arrhenius dependence on temperature [39]. Apart from those, the contact resistance (R_f) is also a function of temperature although the dependence is assumed to be linear. To summarize, the temperature-dependent parameters are modeled by

$$\begin{aligned} K^{\pm}(T) &= K^{\pm}_{\text{ref}} \exp\left(\frac{E^{\pm}_K}{\bar{R}}\left(\frac{1}{T} - \frac{1}{T_{\text{ref}}}\right)\right) \\ D^{\pm}_s(T) &= D^{\pm}_{s,\text{ref}} \exp\left(\frac{E^{\pm}_{Ds}}{\bar{R}}\left(\frac{1}{T} - \frac{1}{T_{\text{ref}}}\right)\right) \\ R_f(T) &= R_{f0} + \alpha T \end{aligned} \tag{5}$$

where T_{ref} is reference temperature, $K^{\pm}_{\text{ref}}$ and $D^{\pm}_{s,\text{ref}}$ are the parameter values at that reference temperature, R_{f0} is the constant part of the contact resistance and α is the proportional constant.

Remark 1. In general, the contact resistance R_f could be a nonlinear function of the temperature. However, the linear dependence of R_f on temperature assumed here will be helpful in simplifying the observer design problem in the next section, Adaptive Observer Design.

In this study, we use the following approximation of the open circuit potential expression [39]:

$$U^{\pm}\left(c^{\pm}_{s,e},T\right) \approx U^{\pm}\left(c^{\pm}_{s,e},T_{\text{ref}}\right) + \frac{\partial U^{\pm}}{\partial T}(T - T_{\text{ref}}) \tag{6}$$

Note that there are some simplifying assumptions taken while developing the SPM. First, the electrolyte dynamics is not taken into account. The solid material charge dynamics is disregarded while the molar flux is averaged. Moreover, the SPM is more suitable for lower charge/discharge rates when the mass and charge transport through the electrolyte are negligible. In recent literature, some improved versions of the SPM are presented which relax some of these aforementioned assumptions and extend the model to be applicable for higher charge/discharge scenarios. In Ref. [42], the electrolyte concentration and potential dynamics are considered by approximating them using polynomial functions. A similar extension is developed in Ref. [43] including nonuniform reaction distribution. In Ref. [44], a seventh-order, enhanced SPM with electrolyte diffusion and temperature-dependent parameters is developed to extend the conventional SPM. Nevertheless, despite the improved predictive capability of these enhanced models, we used the conventional SPM [15,16]; due to its suitability for the analytical adaptive observer designs, we propose here. In any case, it should be emphasized that the conventional SPM is a tradeoff between amounts of electrochemical phenomenon captured and the simplified form needed for observer design and real-time implementation.

Model Reduction and Finite-Dimensional Approximation

The two-electrode SPM discussed in the previous section, Lithium-Ion Cell Electrochemical-Thermal Model, suffers from weak observability of the full state from differential voltage measurement [16]. The common approach to deal with this issue is to approximate Li-ion concentration in the one electrode as an algebraic function of the concentration in another electrode [16,17]. In this paper, we follow the approach in Ref. [17] for model reduction where the positive electrode concentration is considered as an algebraic function of the negative electrode concentration. The purpose of this step is to get an observable model (a single PDE in this case) for observer design. This single PDE describes the negative electrode diffusion dynamics along with a nonlinear output voltage map. Although the fidelity of this reduced model is not as high as other complex models such as P2D, this reduced model is suitable for observer design due to its observability and simpler mathematical structure.

After that the spatial derivatives of the PDE is discretized by finite central difference method while keeping the time derivatives intact. The discretization is illustrated in Fig. 1. The resulting ordinary differential equations are

$$\begin{aligned} \dot{c}_{s0} &= -3ac_{s0} + 3ac_{s1} \\ \dot{c}_{sm} &= \left(1 - \frac{1}{m}\right)ac_{s(m-1)} - 2ac_{sm} + \left(1 + \frac{1}{m}\right)ac_{s(m+1)} \\ \dot{c}_{sM} &= \left(1 - \frac{1}{M}\right)ac_{s(M-1)} - \left(1 - \frac{1}{M}\right)ac_{sM} - \left(1 + \frac{1}{M}\right)bI \end{aligned} \tag{7}$$

with $m = 1,\ldots,(M-1)$, discretization step $\Delta = R/M$, $a = D^-_s/\Delta^2$, $b = 1/a^-_s F\Delta A L^-$. The voltage equation can be derived from Eq. (2) by substituting $c^-_{s,e} = c_{sM}$ and $c^+_{s,e} = k_1 c_{sM} + k_2$ where k_1 and k_2 are constants in the algebraic relationship between positive and negative electrode Li-ion concentrations. These constants can be derived considering $\partial/\partial t(n_{Li}) = 0$ where n_{Li} is the total number of Li-ions [17]. Finally, the output voltage expression is given by

$$\begin{aligned} V = {} & \frac{\bar{R}T}{\alpha^+ F}\sinh^{-1}\left(\frac{I}{2a^+_s AL^+ i^+_0}\right) - \frac{\bar{R}T}{\alpha^- F}\sinh^{-1}\left(\frac{I}{2a^-_s AL^- i^-_0}\right) \\ & + U^+(k_1 c_{sM} + k_2) - U^-(c_{sM}) - R_f(T)I \end{aligned} \tag{8}$$

where the exchange current densities are given by

$$\begin{aligned} i^+_0 &= K^+(T)\sqrt{c_e(k_1 c_{sM} + k_2)\left(c^+_{s,\max} - (k_1 c_{sM} + k_2)\right)} \\ i^-_0 &= K^-(T)\sqrt{c_e c_{sM}\left(c^-_{s,\max} - c_{sM}\right)} \end{aligned} \tag{9}$$

The cell thermal dynamics is used as it is given by Eq. (4).

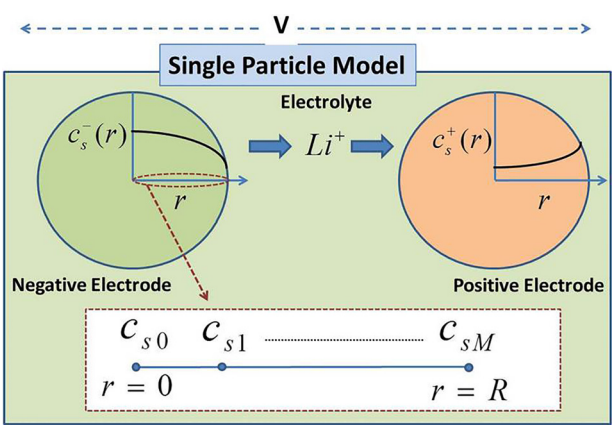

Fig. 1 Illustration of SPM with discretized nodes

Estimation Problem

State-Space Model Formulation and Analysis. The finite-dimensional state-space model for the Li-ion cell can be assembled from Eqs. (7) and (4) along with the output voltage map formed using Eq. (8) and is given as

$$\begin{aligned} \dot{x}_1 &= \theta f_1(x_2) A x_1 + B u \\ \dot{x}_2 &= u f_2(x_{1M}, x_2, y_1) - k(x_2 - x_{2_\infty}) \\ y_1 &= h(x_{1M}, x_2, u) - R_{f0} u - \alpha x_2 u \\ y_2 &= x_2 \end{aligned} \tag{10}$$

where $x_1 = [c_{s1}, \ldots, c_{sM}]^T \in R^M$ is the state vector describing Li-ion concentrations at various nodes, $x_{1M} = x_1(M) = c_{sM} \in R$ is the surface concentration state, $x_2 \in R$ is temperature state and $x_{2_\infty} \in R$ is the coolant/ambient temperature, $\theta = D^-_{s,\text{ref}}/\Delta^2 \in R$ is the scalar parameter related to the diffusion coefficient, $R_{f0} \in R$ is the constant part of the contact resistance, $\alpha \in R$ is the parameter of the temperature-dependent part of the contact resistance, $y_1 \in R$ is the measured voltage, $y_2 \in R$ is the measured temperature, $u \in R$ is the input current, $f_1 : R \to R$ is a scalar function of the temperature given by the exponential term in the Arrhenius equation (5), $A \in R^{M \times M}$ is the tridiagonal matrix formed from Eq. (7), $B = [0, \ldots, 0, B_M]^T \in R^{M \times 1}$ is a column vector formed by Eq. (7) where $B_M = 1/a_s^- F \Delta A L^-$, $f_2 : R^3 \to R$ is a scalar function formed by Eq. (4), $k \in R$ is a scalar parameter, $h : R^3 \to R$ is a scalar function derived from the voltage map (8).

Considering Eq. (7), the zeroth node concentration does not have any contribution in the dynamics of the other nodes. Therefore, inclusion of the zeroth node dynamics results in an unobservable state-space model. The reason behind this lies in the particular structure of the A matrix obtained from the central finite difference discretization of the boundary condition. Moreover, other type of discretization such as forward difference will lead to $c_{s0} = c_{s1}$ making inclusion of c_{s0} dynamics redundant in the state-space model. Consequently, simply dropping the first dynamic equation in Eq. (7), an observable state-space model (10) is obtained. If required, the zeroth node concentration can be approximated from the estimated concentration of the first node using an open-loop observer (just the copy of the plant) based on the first equation in Eq. (7). Moreover, as will be illustrated later, the zeroth node concentration does not contribute to the computation of volume averaged bulk SOC of the cell.

We make the following observations of the system (10).

Observation I: The A matrix in Eq. (10) is negative semidefinite.

Observation II: The functions f_1, f_2, and h are bounded functions and f_1 is positive.

Observation III: The local observability of Eq. (10) can be verified by observability matrix rank condition on linearized version of Eq. (10) at different points of the operating regime [17,24].

Observation IV: The output y_1 is a monotonically increasing function of the surface concentration x_{1M} for a given current and temperature (given in Fig. 2). Therefore, the following fact can be concluded: given any $u = u^*$, $x_2 = x_2^*$, and $R_f = R_f^*$, for two different values $x_{1M}^{(1)}$ and $x_{1M}^{(2)}$, we have $y_1^{(1)} = h^{(1)}\left(x_{1M}^{(1)}, x_2^*, u^*\right) - R_f^* u^*$ and $y_1^{(2)} = h^{(2)}\left(x_{1M}^{(2)}, x_2^*, u^*\right) - R_f^* u^*$. Now, using the monotonically increasing property, we can write that

$$\text{sgn}\left(y_1^{(1)} - y_1^{(2)}\right) = \text{sgn}\left(x_{1M}^{(1)} - x_{1M}^{(2)}\right) \Rightarrow \text{sgn}\left(h^{(1)}\left(x_{1M}^{(1)}, x_2^*, u^*\right) - h^{(2)}\left(x_{1M}^{(2)}, x_2^*, u^*\right)\right) = \text{sgn}\left(x_{1M}^{(1)} - x_{1M}^{(2)}\right)$$

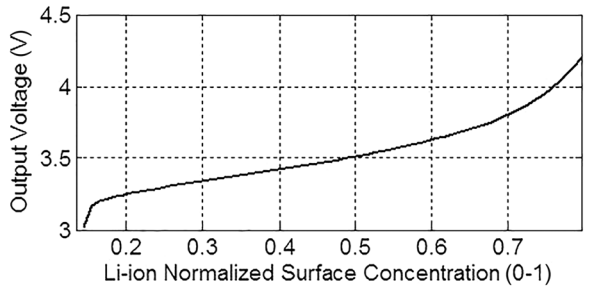

Fig. 2 Output voltage (y_1) as a function of surface concentration (x_{1M})

Estimation Problem Formulation. *State estimation*: The state estimation problem consists of following elements:

Bulk SOC: Bulk SOC represents the available energy in the cell. It can be computed from the full state vector x_1 information using the volume averaging formula

$$\text{SOC}_{\text{Bulk}} = \frac{1}{4\pi R^3 c^-_{s,\max}} \int_0^R 4\pi r^2 c_s^-(r,t)\, dr \tag{11}$$

Surface SOC: Surface SOC represents the power capability of the cell. The state x_{1M} indicates the surface SOC.

Temperature: Note that estimation of temperature state x_2 is optional as we directly measure the cell temperature. However, the estimated temperature can be used as filtered version of the noisy measurement.

Parameter estimation: The parameter estimation problem consists of the following elements:

Diffusion coefficient: This is represented by θ in Eq. (10).

Contact resistance: This is represented by R_f in Eq. (10). Note that R_f has two components: a constant term and a temperature-dependent term. To simplify the observer design process, we assume that the parameter of the temperature dependent term α is known with sufficient accuracy and we concentrate on the estimation of the constant term R_{f0}. The assumption that the parameter α is known with sufficient accuracy essentially helps in reducing the number of unknown parameters to be estimated online. Like other known model parameters, this parameter can be identified a priori by offline identification techniques.

Active material volume fraction of the negative electrode: This is represented by active surface area (a_s^-) as $a_s^- = 3\varepsilon_s/R$, where ε_s is the active material volume fraction. The parameter a_s^- is present in matrix B and function h in Eq. (10). However, sensitivity analysis showed that the error in a_s^- parameter has negligible effect on function h while it has significant impact on the B matrix. Hence, the uncertainty due to a_s^- is assumed to be translated into the parameter B_M which is the last and only nonzero element in B matrix. This is similar to the uncertainty in the boundary input coefficient assumed in Ref. [24].

Apart from improving the accuracy of the state estimates, the estimated information of these parameters can be used as an SOH indicator [40,45].

Adaptive Observer Design

In existing literature, Lyapunov's stability analysis is found to be one of the useful approaches for adaptive observer design [46,47]. In this paper, we adopt a similar approach where the adaptive observer is designed and analyzed via Lyapunov's direct method. The proposed adaptive observer scheme estimates the states (x_1, x_2) and parameters (θ, R_{f0}, B_M) using the measurements (y_1, y_2, u). All the other model parameters and functions are assumed to be known.

The adaptive observer schematic is given in Fig. 3. The structure consists of two observers working in cascade. Observer I estimates the surface concentration $(\hat{x}_{1M})$, temperature $(\hat{x}_2)$, and contact resistance parameter $(\hat{R}_{f0})$ using voltage (y_1) and temperature (y_2) measurement. Observer II estimates the full concentration state vector $(\hat{x}_1)$, diffusion coefficient $(\hat{\theta})$, and B matrix parameter $(\hat{B}_M)$ using the estimates of surface concentration $(\hat{x}_{1M})$ and temperature $(\hat{x}_2)$ from Observer I. Note that, in Observer II, the use of estimated temperature is optional as we have directly

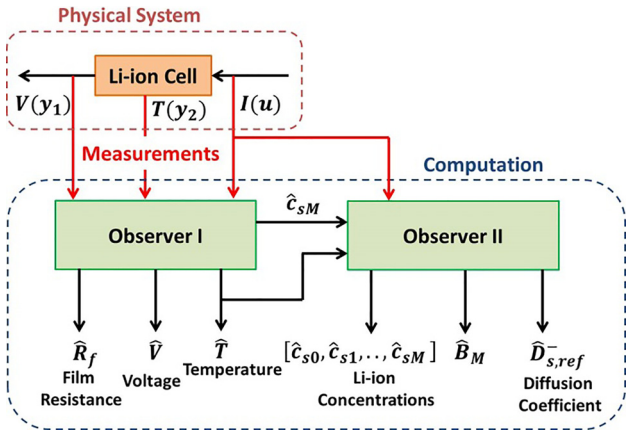

Fig. 3 Adaptive observer scheme

measured temperature. However, we opt to use the estimated temperature which is a filtered version of the noisy measured temperature.

The motivation behind splitting the observer structure into two parts lies in the simplification of the design and tuning. In essence, the full state and parameter vector to be estimated are partitioned into two groups. The first group consists of the surface concentration and temperature, which are directly related to the available measurements (y_1, y_2), and contact resistance, which enters the model as a multiplier to the measured input current; the second group contains the rest of the states and parameters. Then in a cascaded manner, Observer I estimates the first group, and feeds it to Observer II, which subsequently estimates the second group.

Design of Observer I. In the design of Observer I, we concentrate on the following reduced-order system obtained by partitioning the full dynamics given in Eq. (10):

$$\begin{aligned}
\dot{R}_{f0} &= 0 \\
\dot{x}_{1M} &= \theta f_1(x_2)A_1 x_{1(M-1)} + \theta f_1(x_2)A_2 x_{1M} + B_M u \\
\dot{x}_2 &= u f_2(x_{1M}, x_2, y_1) - k(x_2 - x_{2_\infty}) \\
y_1 &= h(x_{1M}, x_2, u) - R_{f0}u - \alpha x_2 u \\
y_2 &= x_2
\end{aligned} \tag{12}$$

where x_{1M} is the surface concentration, $x_{1(M-1)} \in R^{M-1}$ is the rest of the state vector x_1 except x_{1M}, R_{f0} is the unknown parameter, A_1 and A_2 are the partitioned matrices originating from the last row of the x_1 dynamics in Eq. (10). Note that the reduced-order system (12) is an uncertain system due to uncertainties in θ, B_M, and $x_{1(M-1)}$.

The observer structure is given as

$$\begin{aligned}
\dot{\hat{x}}_{1M} &= \bar{\theta} f_1(\hat{x}_2)A_1 \bar{x}_{1(M-1)} + \bar{\theta} f_1(\hat{x}_2)A_2 \hat{x}_{1M} + \bar{B}_M u + L_1(y_1 - \hat{y}_1) \\
\dot{\hat{x}}_2 &= u f_2(\hat{x}_{1M}, \hat{x}_2, y_1) - k(\hat{x}_2 - x_{2_\infty}) + L_2(y_2 - \hat{y}_2) \\
\hat{y}_1 &= h(\hat{x}_{1M}, \hat{x}_2, u) - \hat{R}_{f0}u - \alpha \hat{x}_2 u \\
\hat{y}_2 &= \hat{x}_2
\end{aligned} \tag{13}$$

where $\bar{\theta}$ and $\bar{B}_M$ are constant (guessed or nominal) values, and $\bar{x}_{1(M-1)}$ is the partitioned state vector obtained from the open-loop model without any measurement feedback. The observer error dynamics can be written as

$$\begin{aligned}
\dot{\tilde{x}}_{1M} &= F_1 - L_1 \tilde{y}_1 \\
\dot{\tilde{x}}_2 &= u\tilde{f}_2 - k\tilde{x}_2 - L_2 \tilde{y}_2 \\
\tilde{y}_1 &= \tilde{h} - \tilde{R}_{f0}u - \alpha \tilde{x}_2 u \\
\tilde{y}_2 &= \tilde{x}_2
\end{aligned} \tag{14}$$

where $F_1 = \theta f_1(x_2)A_1 x_{1(M-1)} + \theta f_1(x_2)A_2 x_{1M} - \bar{\theta} f_1(\hat{x}_2)A_1 \bar{x}_{1(M-1)} - \bar{\theta} f_1(\hat{x}_2)A_2 \hat{x}_{1M} + (B_M - \bar{B}_M)u$, $\tilde{h} = h(x_{1M}, x_2, u) - h(\hat{x}_{1M}, \hat{x}_2, u)$, $\tilde{f}_2 = f_2(x_{1M}, x_2, y_1) - f_2(\hat{x}_{1M}, \hat{x}_2, y_1)$, $\tilde{R}_f = R_f - \hat{R}_f$, $\tilde{x}_1 = x_1 - \hat{x}_1$, $\tilde{x}_2 = x_2 - \hat{x}_2$, $\tilde{y}_1 = y_1 - \hat{y}_1$, $\tilde{y}_2 = y_2 - \hat{y}_2$, and L_1, L_2 are observer gains to be determined.

The following Lyapunov function candidate is chosen to analyze the convergence of error dynamics:

$$V = \frac{1}{2}\tilde{x}_{1M}^2 + \frac{1}{2}\tilde{x}_2^2 + \frac{1}{2}\tilde{R}_{f0}^2$$

The derivative of the Lyapunov function candidate is given as

$$\begin{aligned}
\dot{V} &= \tilde{x}_{1M}\dot{\tilde{x}}_{1M} + \tilde{x}_2\dot{\tilde{x}}_2 + \tilde{R}_{f0}\dot{\tilde{R}}_{f0} \\
&\Rightarrow \dot{V} = \tilde{x}_{1M}(F_1 - L_1\tilde{y}_1) + \tilde{x}_2\left(u\tilde{f}_2 - k\tilde{x}_2 - L_2\tilde{y}_2\right) - \tilde{R}_{f0}\dot{\tilde{R}}_{f0} \\
&\Rightarrow \dot{V} = \tilde{x}_{1M}\left(F_1 - L_1\left(\tilde{h} - \tilde{R}_{f0}u - \alpha\tilde{x}_2 u\right)\right) \\
&\qquad + \tilde{x}_2\left(u\tilde{f}_2 - k\tilde{x}_2 - L_2\tilde{y}_2\right) - \tilde{R}_{f0}\dot{\tilde{R}}_{f0} \\
&\Rightarrow \dot{V} = \tilde{x}_{1M}\left(F_1 - L_1\tilde{h}\right) + L_1\tilde{x}_{1M}\tilde{R}_{f0}u + \tilde{x}_2\left(u\tilde{f}_2 + L_1\alpha\tilde{x}_{1M}u - k\tilde{x}_2\right. \\
&\qquad \left. - L_2\tilde{y}_2\right) - \tilde{R}_{f0}\dot{\tilde{R}}_{f0}
\end{aligned}$$

From Observation IV, we can write that $\mathrm{sgn}(\tilde{h}) = \mathrm{sgn}(\tilde{x}_{1M})$ which implies that $\tilde{x}_{1M}\tilde{h} > 0$ or equivalently, $\tilde{x}_{1M}\tilde{h} = |\tilde{x}_{1M}||\tilde{h}|$.

Remark 2. Here, $\tilde{h} = h(x_{1M}, x_2, u) - h(\hat{x}_{1M}, \hat{x}_2, u)$ is not only an implicit function of $\tilde{x}_{1M}$ but also an implicit function of $\tilde{x}_2$. However, h is much less sensitive to temperature x_2 than the surface concentration x_{1M}. Moreover, we have temperature measurement available which means $\tilde{x}_2$ will always have negligible effect on $\tilde{h}$. Therefore, we can reasonably apply Observation IV in the present scenario even when $\tilde{x}_2 \neq 0$ identically.

Based on the above argument and $\tilde{y}_2 = \tilde{x}_2$, $\dot{V}$ can be written as

$$\begin{aligned}
\dot{V} &= \left(\tilde{x}_{1M}F_1 - L_1|\tilde{x}_{1M}||\tilde{h}|\right) + \left(u\tilde{f}_2\tilde{x}_2 + L_1\alpha\tilde{x}_2\tilde{x}_{1M}u - (k + L_2)\tilde{x}_2^2\right) \\
&\quad + L_1\tilde{x}_{1M}\tilde{R}_{f0}u - \tilde{R}_{f0}\dot{\tilde{R}}_{f0}
\end{aligned}$$

Using the inequality, $ab \leq |ab| = |a||b|$

$$\begin{aligned}
\dot{V} &\leq \left(|\tilde{x}_{1M}||F_1| - L_1|\tilde{x}_{1M}||\tilde{h}|\right) + \left(|u\tilde{f}_2||\tilde{x}_2| + |L_1\alpha\tilde{x}_{1M}u||\tilde{x}_2|\right. \\
&\quad \left. - (k + L_2)|\tilde{x}_2|^2\right) + L_1\tilde{x}_{1M}\tilde{R}_{f0}u - \tilde{R}_{f0}\dot{\tilde{R}}_{f0} \\
&\Rightarrow \dot{V} \leq |\tilde{x}_{1M}|\left(|F_1| - L_1|\tilde{h}|\right) + |\tilde{x}_2|\left(|u\tilde{f}_2| + |L_1\alpha\tilde{x}_{1M}u|\right. \\
&\quad \left. -(k + L_2)|\tilde{x}_2|\right) + L_1\tilde{x}_{1M}\tilde{R}_{f0}u - \tilde{R}_{f0}\dot{\tilde{R}}_{f0}
\end{aligned}$$

Now, the following adaptive law is chosen for the estimation of contact resistance:

$$\begin{aligned}
\dot{\tilde{R}}_{f0} &= -L_3\mathrm{sgn}(u)\mathrm{sgn}(\tilde{y}_1) \Rightarrow \dot{\tilde{R}}_{f0} \\
&= -L_3\mathrm{sgn}(u)\mathrm{sgn}\left(\tilde{h} - \tilde{R}_{f0}u - \alpha\tilde{x}_2 u\right)
\end{aligned}$$

Consequently, the $\dot{V}$ equation can be written as

$$\begin{aligned}
\dot{V} &\leq |\tilde{x}_{1M}|\left(|F_1| - L_1|\tilde{h}|\right) + |\tilde{x}_2|\left(|u\tilde{f}_2| + |L_1\alpha\tilde{x}_{1M}u| - (k + L_2)|\tilde{x}_2|\right) \\
&\quad + L_1\tilde{x}_{1M}\tilde{R}_{f0}u + L_3\tilde{R}_{f0}\mathrm{sgn}(u)\mathrm{sgn}\left(\tilde{h} - \tilde{R}_{f0}u - \alpha\tilde{x}_2 u\right)
\end{aligned} \tag{15}$$

In the first term on the right-hand side of Eq. (15), for a sufficiently high $L_1 > |F_1|/|\tilde{h}|$, $|\tilde{x}_{1M}|\left(|F_1| - L_1|\tilde{h}|\right)$ will be negative. This means that $|\tilde{x}_{1M}|$ will always decrease till this condition $L_1 > |F_1|/|\tilde{h}|$ is true. However, $\tilde{x}_{1M}$ will not go to zero. It will stay on a bounded manifold in the error space determined by the value of L_1 and the magnitude of $|F_1|$.

Similarly, we can analyze the second term in right-hand side of Eq. (15). Due to some preselected high positive L_2, $|\tilde{x}_2|$ will

decrease until the condition $L_2 > \left(\left|u\tilde{f}_2\right| + |L_1\alpha\tilde{x}_{1M}u|\right)/|\tilde{x}_2|$ is true. Consequently, $|\tilde{x}_2|$ will stay on some bounded manifold in the error space determined by the value of L_2 and magnitude of $\left(\left|u\tilde{f}_2\right| + |L_1\alpha\tilde{x}_{1M}u|\right)$.

Next, we consider the third and fourth term on the right-hand side of Eq. (15). After convergence of the second term, the steady-state error $\tilde{x}_{2-ss}$ is negligible. Then, under the condition $\left|\tilde{h}\right| < \left|\tilde{R}_{f0}u\right|$, we can write $\text{sgn}\left(\tilde{h} - \tilde{R}_{f0}u - \alpha\tilde{x}_{2-ss}u\right) = \text{sgn}\left(-\tilde{R}_{f0}u\right) = -\text{sgn}\left(\tilde{R}_{f0}\right)\text{sgn}(u)$. Consequently, the third and fourth term becomes $L_1\tilde{x}_{1M}\tilde{R}_{f0}u - L_3\tilde{R}_{f0}\text{sgn}\left(\tilde{R}_{f0}\right)$. Then with the use of the inequality, $ab \le |ab| = |a||b|$, the above expression becomes $\left|\tilde{R}_{f0}\right|(L_1|\tilde{x}_{1M}||u| - L_3)$. For some preselected high positive L_3 will make $\left|\tilde{R}_{f0}\right|$ to decrease till one of the two conditions $L_1|\tilde{x}_{1M}||u| < L_3$ or $\left|\tilde{h}\right| < \left|\tilde{R}_{f0}u\right|$ is true. Subsequently, $\left|\tilde{R}_{f0}\right|$ will decrease and stay on some bounded manifold in the error space determined by the values of L_3, L_1, and magnitude of $|\tilde{x}_{1M}|$ and $\left|\tilde{h}\right|$.

This Lyapunov analysis concludes that for some high observer gains, the errors $\tilde{x}_{1M}$, $\tilde{x}_2$, and $\tilde{R}_{f0}$ will go to some bounded manifold. For sufficiently high values of L_1 and L_2, the steady-state value of $\tilde{x}_{1M}$ and $\tilde{x}_2$ can be made negligibly small for all practical purposes. Next, the estimates $\hat{x}_{1M}$ and $\hat{x}_2$ will be used by Observer II with the assumption of negligible steady-state values of error variables $\tilde{x}_{1M}$ and $\tilde{x}_2$.

Remark 3. The convergence of the estimate of the contact resistance ($\hat{R}_{f0}$) requires nonzero input current ($u \neq 0$). This is also evident from Eq. (12) as the contact resistance enters into the output equation as multiplied by the current ($R_{f0}u$).

Design of Observer II. In the design of Observer II the whole Li-ion concentration dynamics of x_1 with unknown parameters θ and B_M are considered. This partial dynamics is given as

$$\begin{aligned} \dot{\theta} &= 0 \\ \dot{B}_M &= 0 \\ \dot{x}_1 &= \theta f_1(x_2)Ax_1 + [0,\ldots,0,B_M]^T u \\ y_{1M} &= x_{1M} = Cx_1 \text{ where } C = [0,\ldots,0,1] \end{aligned} \tag{16}$$

where x_1 is the whole Li-ion concentration vector, θ and B_M are the unknown parameters, temperature x_2 is the estimate from Observer I and y_{1M} is the estimated surface concentration from Observer I. We assume that the steady-state error is negligible in both the estimates due to a proper selection of gains in Observer I.

The observer structure is given as

$$\begin{aligned} \dot{\hat{x}}_1 &= \hat{\theta}f_1(x_2)A\hat{x}_1 + [0,.,0,\hat{B}_M]^T u + L_4(y_{1M} - \hat{y}_{1M}) \\ \hat{y}_{1M} &= C\hat{x}_1 \end{aligned} \tag{17}$$

The observer error dynamics can be written as

$$\begin{aligned} \dot{\tilde{x}}_1 &= \theta f_1(x_2)Ax_1 - \hat{\theta}f_1(x_2)A\hat{x}_1 + [0,.,0,\hat{B}_M]^T u - L_4 \\ \tilde{y}_{1M}\tilde{y}_{1M} &= C\tilde{x}_1 \end{aligned} \tag{18}$$

The following Lyapunov function candidate is chosen to analyze the convergence of the error dynamics:

$$V = \frac{1}{2}\tilde{x}_1^T\tilde{x}_1 + \frac{1}{2}K_1\tilde{\theta}^2 + \frac{1}{2}K_2\tilde{B}_M^2 \quad \text{with } (K_1, K_2 > 0) \tag{19}$$

The derivative of the Lyapunov function candidate can be written as (we drop the argument of the function f_1 for brevity)

$$\begin{aligned} \dot{V} &= \tilde{x}_1^T\dot{\tilde{x}}_1 + K_1\tilde{\theta}\dot{\tilde{\theta}} + K_2\tilde{B}_M\dot{\tilde{B}}_M \\ \Rightarrow \dot{V} &= \tilde{x}_1^T\left(\theta f_1 Ax_1 - \hat{\theta}f_1 A\hat{x}_1 - L_4\tilde{y}_{1M}\right) + \tilde{x}_1^T[0,..,\tilde{B}_M]^T u \\ &\quad + K_1\tilde{\theta}\dot{\tilde{\theta}} + K_2\tilde{B}_M\dot{\tilde{B}}_M \\ \Rightarrow \dot{V} &= \tilde{x}_1^T\left(\theta f_1 A\tilde{x}_1 + \tilde{\theta}f_1 A\hat{x}_1 - L_4 C\tilde{x}_1\right) + \tilde{y}_{1M}\tilde{B}_M u + K_1\tilde{\theta}\dot{\tilde{\theta}} \\ &\quad + K_2\tilde{B}_M\dot{\tilde{B}}_M \\ \Rightarrow \dot{V} &= \theta f_1\tilde{x}_1^T A\tilde{x}_1 - \tilde{x}_1^T L_4 C\tilde{x}_1 + \tilde{x}_1^T\tilde{\theta}f_1 A\hat{x}_1 + K_1\tilde{\theta}\dot{\tilde{\theta}} + \tilde{y}_{1M}\tilde{B}_M u \\ &\quad + K_2\tilde{B}_M\dot{\tilde{B}}_M \end{aligned}$$

Considering slowly varying parameters ($\dot{\theta}, \dot{B}_M = 0$)

$$\begin{aligned} \dot{V} &= \left(\theta f_1\tilde{x}_1^T A\tilde{x}_1 - \tilde{x}_1^T L_4 C\tilde{x}_1\right) + \tilde{\theta}\left(f_1\hat{x}_1^T A^T\tilde{x}_1 - K_1\dot{\hat{\theta}}\right) \\ &\quad + \tilde{B}_M\left(\tilde{y}_{1M}u - K_2\dot{\hat{B}}_M\right) \end{aligned} \tag{20}$$

Next, the following adaptation laws are chosen:

$$\begin{aligned} \dot{\hat{B}}_M &= u\tilde{y}_{1M}/K_2 \\ \dot{\hat{\theta}} &= L_5\tilde{y}_{1M}/K_1 \end{aligned} \tag{21}$$

where L_5 is to be determined. With the choice of these adaptation laws, the third term on right-hand side of Eq. (20) vanishes. Considering the second term on right-hand side of Eq. (20)

$$\begin{aligned} \tilde{\theta}\left(f_1\hat{x}_1^T A^T\tilde{x}_1 - L_5\tilde{y}_{1M}\right) &= \tilde{\theta}\left(f_1\hat{x}_1^T A^T\tilde{x}_1 - L_5 C\tilde{x}_1\right) \\ &= \left(f_1\hat{x}_1^T A^T - L_5 C\right)\tilde{x}_1\tilde{\theta} \end{aligned}$$

To vanish the second term in Eq. (20), the following condition needs to be satisfied:

$$f_1\hat{x}_1^T A^T = L_5 C \Rightarrow f_1\hat{x}_1^T A^T C^T = L_5 CC^T \Rightarrow L_5 = f_1\hat{x}_1^T A^T C^T, \text{ as } CC^T = 1$$

Consequently, the second adaptation law in Eq. (21) becomes

$$\dot{\hat{\theta}} = \frac{f_1\hat{x}_1^T A^T C^T\tilde{y}_{1M}}{K_1} \tag{22}$$

With the choice of these adaptation laws, the Lyapunov function derivative becomes

$$\dot{V} = \left(\theta f_1\tilde{x}_1^T A\tilde{x}_1 - \tilde{x}_1^T L_4 C\tilde{x}_1\right) \tag{23}$$

The observer gain L_4 is chosen such that L_4C becomes positive semidefinite leading to $-\tilde{x}_1^T L_4 C\tilde{x}_1 \le 0$. Note that the matrix L_4C cannot be negative definite due to the structure of the vector C. Using Observation I which states that A is negative semidefinite, we can conclude that $\theta f_1\tilde{x}_1^T A\tilde{x}_1 \le 0$ as the function f_1 and parameter θ are always positive from their physical properties. From this analysis, it can be concluded that $\dot{V} = -\tilde{x}_1^T\beta\tilde{x}_1 \le 0$ where $\beta = \theta f_1 A - L_4 C$. Hence, the boundedness of the estimation errors $\tilde{x}_1$, $\tilde{\theta}$, and $\tilde{B}_M$ is proved. Further, the asymptotic convergence of the errors to zero is analyzed next using a "Lyapunov-like" analysis based on Barbalat's lemma [48,49].

Asymptotic Convergence of $\tilde{x}_1$. In this section, it will be shown that $\dot{V} \to 0$ as $t \to \infty$. Note that the Lyapunov function V is lower-bounded by choice and $\dot{V} \le 0$ is proved in the previous analysis. Uniform continuity of $\dot{V}$ is equivalent to boundedness of $\ddot{V}$ which can be written as

$$\begin{aligned} &\ddot{V} = -2\tilde{x}_1^T\beta\dot{\tilde{x}}_1, \text{ where} \\ &\dot{\tilde{x}}_1 = \theta f_1(x_2)Ax_1 - \hat{\theta}f_1(x_2)A\hat{x}_1 + \left[0,\ldots,0,\tilde{B}_M\right]^T u - L_4 C\tilde{x}_1 \end{aligned}$$

Note that x_1, θ, and f_1 all are bounded from the physical properties of the system. Moreover, input u is also considered to be bounded. From Lyapunov analysis in the previous section, Design of Observer II, it is concluded that $\tilde{x}_1$, $\tilde{\theta}$, and $\tilde{B}_M$ are bounded. Therefore, $\hat{x}_1$ and $\hat{\theta}$ are also bounded. So, it can be concluded that $\dot{\tilde{x}}_1$ is bounded which in turn concludes the boundedness of $\dot{V}$. Hence, it can be concluded using Barbalat's lemma that $\dot{V} \to 0$ as $t \to \infty$. Then, using $\dot{V}$ expression (23), it can be shown that $\tilde{x}_1 \to 0$ as $t \to \infty$.

Asymptotic Convergence of $\tilde{\theta}$ and $\tilde{B}_M$. In this section, it will be shown that $\dot{\tilde{x}}_1 \to 0$ as $t \to \infty$. It is already shown in the previous section, Asymptotic Convergence of $\tilde{x}_1$, that $\tilde{x}_1 \to 0$ as $t \to \infty$. The limit $\int_0^\infty \dot{\tilde{x}}_1 dt = \lim_{t\to\infty} \tilde{x}_1(t) - \tilde{x}_1(0) = -\tilde{x}_1(0)$ exists and is finite. With the signals already shown bounded in the previous step and additionally assuming $\dot{u}$ bounded, the boundedness of $\ddot{\tilde{x}}_1$ can be concluded. Hence, using Barbalat's lemma, it can be concluded that $\dot{\tilde{x}}_1 \to 0$ as $t \to \infty$. Considering the $\dot{\tilde{x}}_1$ expression with $\tilde{x}_1 \to 0$, $\dot{\tilde{x}}_1 = \tilde{\theta} f_1(x_2) A x_1 + \left[0, \ldots, 0, \tilde{B}_M\right]^T u$. As $\dot{\tilde{x}}_1 \to 0$, the above expression boils down to

$$\begin{aligned}
&\tilde{\theta} f_1(x_2) A x_1 + \left[0, \ldots, 0, \tilde{B}_M\right]^T u = 0 \\
&\Rightarrow f_1(x_2) A x_1 \tilde{\theta} + [0, \ldots, 0, u]^T \tilde{B}_M = 0 \\
&\Rightarrow \begin{bmatrix} f_1(x_2) A x_1 \end{bmatrix} \quad [0, \ldots, 0, u]^T \Big]_{M\times 2} \begin{bmatrix} \tilde{\theta} \\ \tilde{B}_M \end{bmatrix}_{2\times 1} = 0 \\
&\Rightarrow X_{M\times 2} \begin{bmatrix} \tilde{\theta} \\ \tilde{B}_M \end{bmatrix}_{2\times 1} = 0, \text{ with } X = \begin{bmatrix} f_1(x_2) A x_1 \end{bmatrix} \quad [0, \ldots, u]^T \Big] \\
&\Rightarrow \left[X^T X\right]_{2\times 2} \begin{bmatrix} \tilde{\theta} \\ \tilde{B}_M \end{bmatrix}_{2\times 1} = 0
\end{aligned}$$

Finally, it can be concluded that $\tilde{\theta}, \tilde{B}_M \to 0$ as $t \to \infty$ under the condition $|X^T X| \neq 0$, which in turn leads to the condition $u \neq 0$. Note that the convergence of the parameter estimates to their true values requires nonzero input current.

Remark 4. The asymptotic convergence analysis of $\tilde{x}_1$, $\tilde{\theta}$, and $\tilde{B}_M$ is built on the assumption that Observer I provides sufficiently accurate estimates of the surface concentration and temperature. However, as there will always be a steady-state error in the estimates of Observer I in reality, $\tilde{x}_1$, $\tilde{\theta}$, and $\tilde{B}_M$ will converge to finite nonzero steady-state values. Moreover, one of the important assumptions for the convergence of $\tilde{\theta}$ and $\tilde{B}_M$ is the boundedness of the $\dot{u}$, which is the derivative of the input current. To comply with this assumption, in real-time implementations of the observer, an input current rate limiter should be used to retain satisfactory performance of the observer.

Systematic Approach for Selection of Observer Gains. As evident in the previous analysis, observer gains selection is of critical importance in this proposed adaptive observer scheme. In this section, a systematic approach is provided for selecting the observer gains.

Observer I:
Step I:

— Select a high positive gain L_1.
— Then select a high gain L_3 satisfying the condition $L_1 |\tilde{x}_{1M}|_{\max} |u|_{\max} < L_3$, where $|u|_{\max}$ is the maximum possible current and $|\tilde{x}_{1M}|_{\max}$ is the allowable value of state error.
— Note the convergence rate and steady-state errors in $\tilde{x}_{1M}$ and $\tilde{R}_{f0}$. Increase gain L_1 and L_3 meeting the condition $L_1 |\tilde{x}_{1M}|_{\max} |u|_{\max} < L_3$ until acceptable convergence rates and steady-state errors are achieved. However, the designer should keep in mind the possible tradeoff between measurement noise amplification and acceptable steady-state error due to high observer gains.

Step II:

— The gain L_2 can be selected independently of other gains. After initializing L_2 to a high value, increase it until an acceptable convergence rate and steady-state error is achieved.

Observer II:
Step III:

— Select a high $L_4 = \sigma[1, .., 1]^T$ with $\sigma > 0$ such that $L_4 C$ is positive semidefinite. Keep increasing σ until an acceptable convergence rate and steady-state error is achieved for $\tilde{x}_1$.

Step IV:

— For a given selection of L_4, the gains K_1 and K_2 for the parameter update laws should be tuned together. These two gains are observed to have a strong interdependence due to the presence of these corresponding parameters in the same dynamic equation. After initializing K_1 and K_2 with arbitrary small positive numbers, keep increasing them until acceptable convergence rates are achieved. Note that proper care should be taken such that the selection of K_1 and K_2 should not significantly impact the $\tilde{x}_1$ convergence.

Simulation Studies

In this section, we demonstrate the performance of the adaptive observer scheme via simulation studies. In this study, the two-electrode SPM is used as the plant model. Model parameter values of Li-ion cell have been taken from Refs. [11,39]. The cell has the following characteristics: Metal oxide positive electrode, graphite negative electrode, cell capacity 6 Ah. To emulate a realistic scenario, 10 mA, 10 mV, and 1 °C variance noise is added to the current, voltage, and temperature measurement, respectively. The state and parameter estimates in the observers are initialized with different initial conditions than that of actual plant. The estimation performance is shown in Figs. 4–6 for a urban dynamometer driving cycle (UDDS). UDDS is originally a velocity profile for testing a full-size (electric) vehicle, from which a scaled-down current profile is constructed.

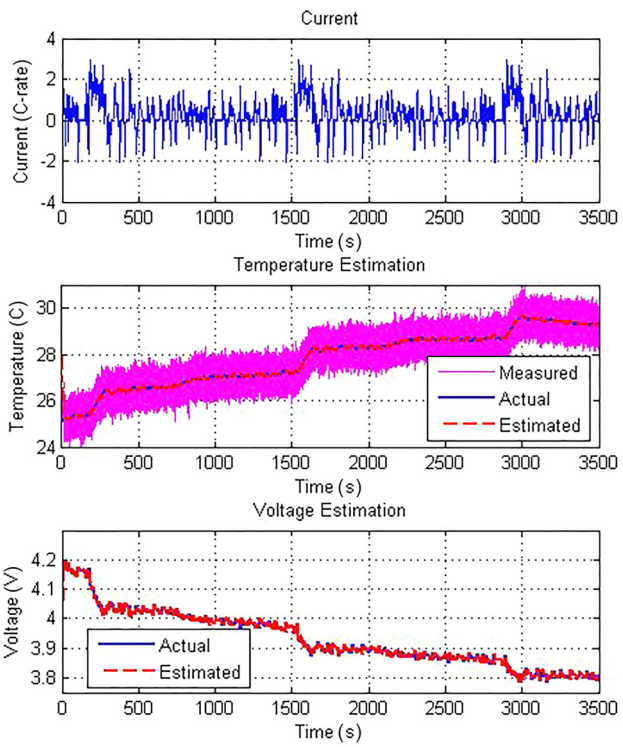

Fig. 4 Temperature and voltage estimation performance

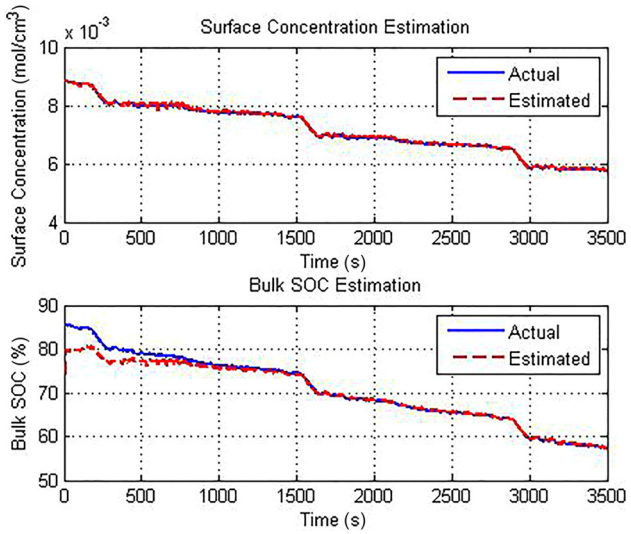

Fig. 5 Bulk SOC and surface concentration estimation performance

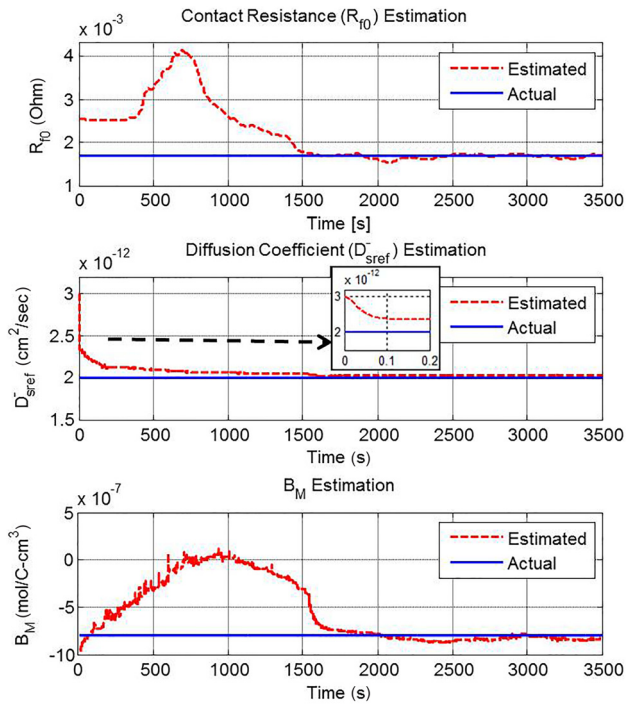

Fig. 6 Parameter estimation performance

From Figs. 4–6, it can be concluded that the state and parameter estimates converge with a reasonable accuracy. Note that the convergence rates for the parameter estimates are much slower than those of the states. However, this should not be a problem due to the time scale separation between states and parameters dynamics.

Experimental Results

In this section, experimental results are shown for the adaptive observer scheme applied to a commercial high power 2.3 Ah $LiFePO_4$–Graphite cell. In the experimental studies, some of the model parameters of Eq. (10) have been identified using experimental data of voltage, current, and temperature while others were adopted from available literature for this particular cell. Although the exchange current densities ($i_0^{\pm}$) in Eq. (3) are generally a function of Li-ion concentrations, we follow the assumption of constant exchange current densities taken in some existing works [41,50,51] to simplify the model identification process. For model identification, we solved a nonlinear least square optimization problem to obtain the parameter set that gives the best fit between experimental and model data. The main model parameters are given in Table 1.

Similar to the simulation studies, the state and parameter estimates are initialized with incorrect initial conditions to evaluate the error convergence of the observers. Then, the evolution of the estimated variables with time is compared to the actual variables.

Remark 5. The only variables that are measured experimentally are the voltage, current, and temperature. Therefore, the "actual" voltage and temperature is the experimentally measured voltage and temperature. To compute the actual bulk SOC, coulomb-counting technique is used. This is possible because of the sufficiently accurate current measurement as mentioned in Ref. [12]. The actual surface SOC evolution is taken from the model which is initialized using the fitted experimental data. The actual parameters of contact resistance, diffusion coefficient, and B_M are also taken from the fitted experimental data by offline system identification. The presented "validation" for these variables (which are not measured in real-time) should therefore be taken with care: It is only meant to show that the estimates from the observers are converged to reasonable values in various experiments. Complete validation of the observers' performance requires additional in situ measurements (such as neutron imaging [54]) and can be considered as a future extension of this work.

Two sets of experimental studies have been performed based on two different current profiles. In the first study, a constant current discharge 2C is used. The results for this study are given in Fig. 7 (voltage and temperature estimation), Fig. 8 (surface and bulk SOC), and Fig. 9 (parameter estimation). As expected, the estimated variables converged to a bounded error ball starting with incorrect initialization. Note that the voltage and temperature estimates have almost negligible steady-state error as should be expected given the measured output variables involve the same states. However, the steady-state error of the unmeasured states and of the parameter estimates is relatively larger.

In the second experimental study, a pulse discharge profile is applied to the cell. The results for this study are given in Figs. 10 (voltage and temperature estimation), 11 (surface and bulk SOC), and 12 (parameter estimation), respectively. Similar to the first experimental study, the estimated variables converged to a bounded error ball starting with incorrect initialization.

Table 1 Model parameters ("*F*" denotes fitted values)

Parameters	Values
$D^-_{s,\mathrm{ref}}$	$2.4 \times 10^{-15}\,\mathrm{m^2/s}$ (F)
i_0^+	$0.0036\,\mathrm{A/m^2}$ (F)
i_0^-	$0.6102\,\mathrm{A/m^2}$ (F)
R_f	$0.0532\,\Omega$ (F)
k_1	-0.9442 (F)
k_2	$22,799\,\mathrm{mol/m^3}$ (F)
a_s^-	$3.48 \times 10^5\,\mathrm{m^2/m^3}$ [50]
ε_s^-	0.58 [41]
R^-	$5 \times 10^{-6}\,\mathrm{m}$ [50]
A	$0.18\,\mathrm{m^2}$ [50]
L^-	$3.4 \times 10^{-5}\,\mathrm{m}$ [50]
$c^+_{s,\max}$	$22,806\,\mathrm{mol/m^3}$ [52]
$c^-_{s,\max}$	$30,555\,\mathrm{mol/m^3}$ [53]
ρv	0.07 kg [50]
C_p	$1100\,\mathrm{J/kg\,K}$ [50]
hA	$0.07\,\mathrm{W/K}$ (F)

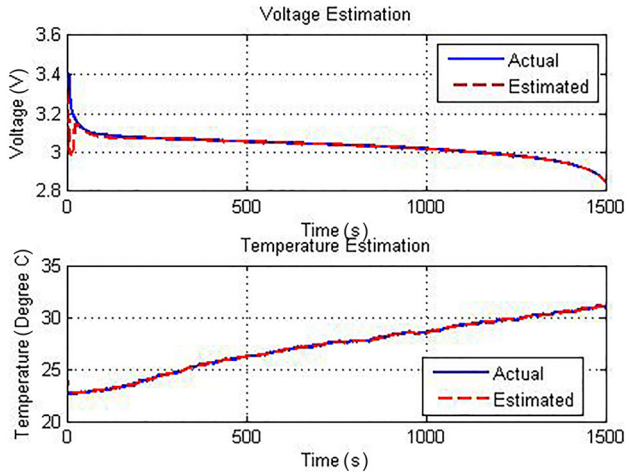

Fig. 7 Voltage and temperature estimation performance for 2C constant discharge profile

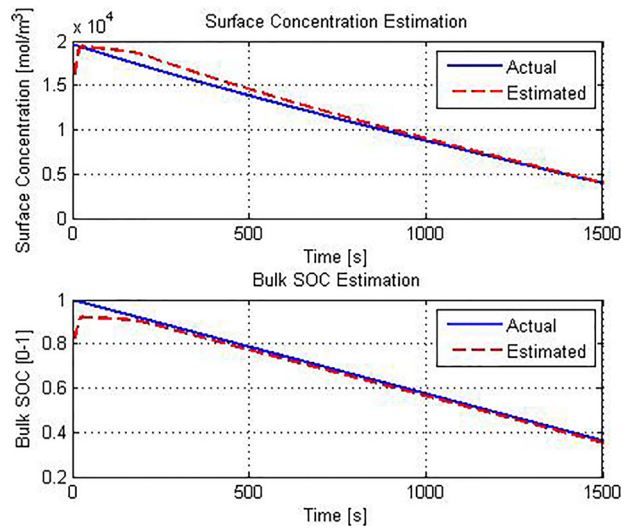

Fig. 8 Surface and bulk SOC estimation performance for 2C constant discharge profile

Limitations of the Proposed Scheme

From the simulation and experimental studies, it is observed that the adaptive observer scheme performs reasonably well in estimating states and parameters. However, there are some limitations of the proposed scheme. In this section, the following shortcomings of the scheme are discussed and illustrated.

Effect of Modeling Uncertainties. In the proposed adaptive observer scheme, uncertainties from unmodeled dynamics/processes are not taken into account explicitly in the design phase. If such uncertainties are present in the state dynamic equations, the effect of the uncertainties can be suppressed to a certain extent using high gains in the observers. However, high gains can amplify the output uncertainties such as measurement noise. Therefore, there is a tradeoff between rejecting the uncertainties in state dynamics and amplifying measurement noise. Moreover, in the presence of high output uncertainties (other than measurement noise), which originate from the unmodeled phenomena in the output equations (e.g., uncertainties in Bulter–Volmer kinetics, overpotentials, etc), the performance of the adaptive scheme degrades significantly.

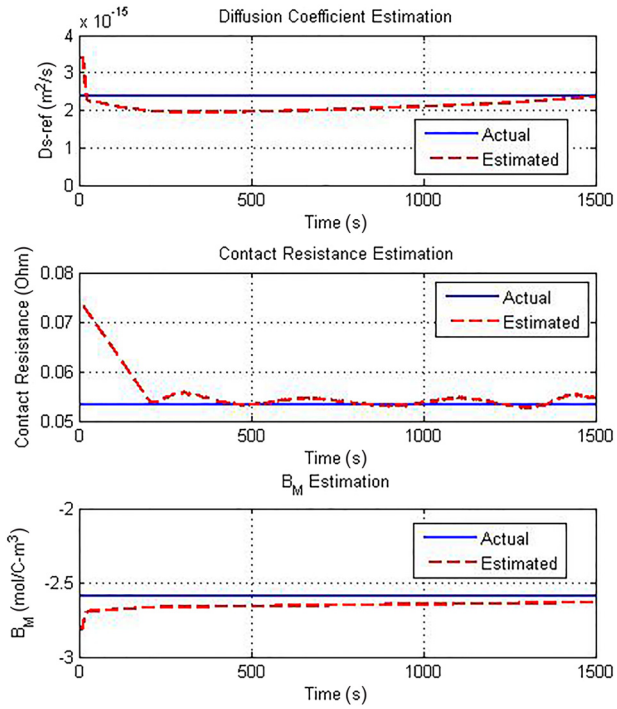

Fig. 9 Parameter estimation performance for 2C constant discharge profile

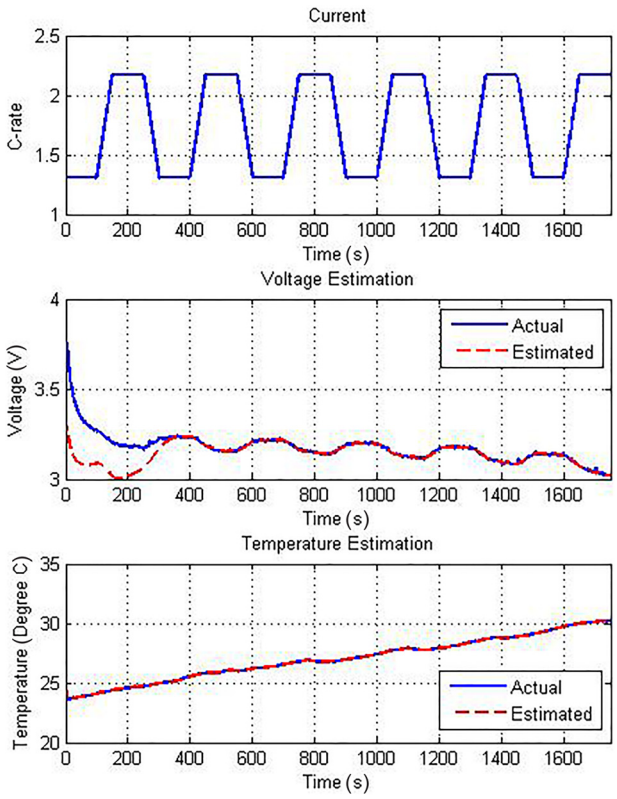

Fig. 10 Applied current, voltage, and temperature estimation performance for pulse discharge profile

The effect of the two aforementioned cases of high output uncertainty and zero input current is tested experimentally. Figure 14 shows that at 1550 s, the input current goes to zero. After the input current goes to zero, the open-loop model voltage

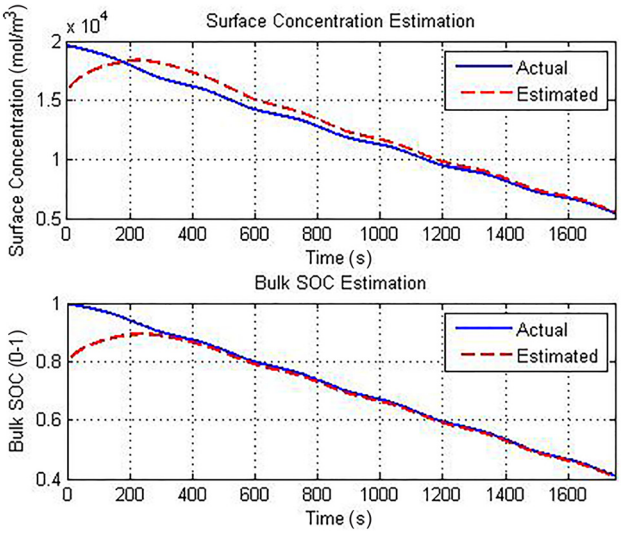

Fig. 11 Surface and bulk SOC Estimation performance for pulse discharge profile

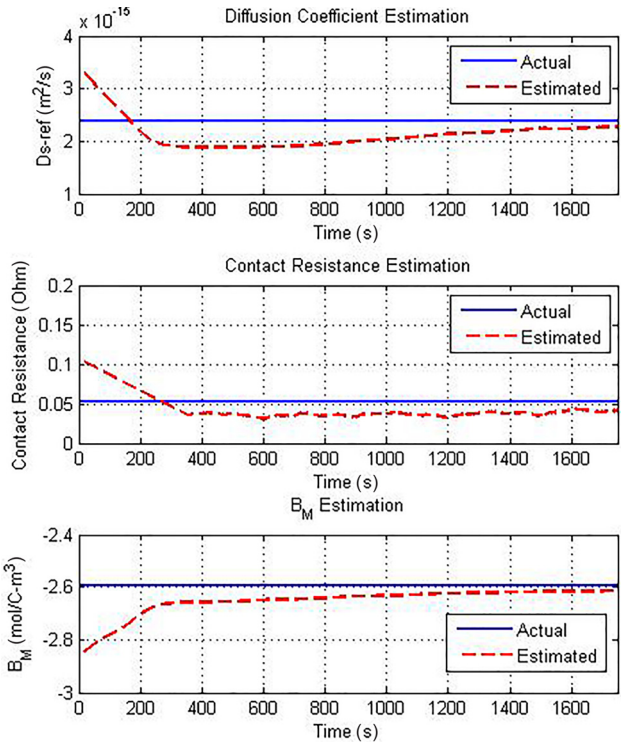

Fig. 12 Parameter estimation performance for pulse discharge profile

cannot track the actual voltage, which is evident from the second subplot of Fig. 14. This indicates the presence of high output uncertainty where the model output has a significant deviation from the actual output. Due to the effect of the high output uncertainty, the estimates of the states and the parameters started diverging after 1550 s which is shown in the third subplot of Fig. 14. Therefore, this illustration shows that the scheme loses its effectiveness under the aforementioned scenarios. Another fact noted from this illustration is that like other estimation algorithms, persistence of excitation is required for the convergence of the estimates for this proposed approach. This fact is observed in this illustration where in case of zero applied current the convergence is poor.

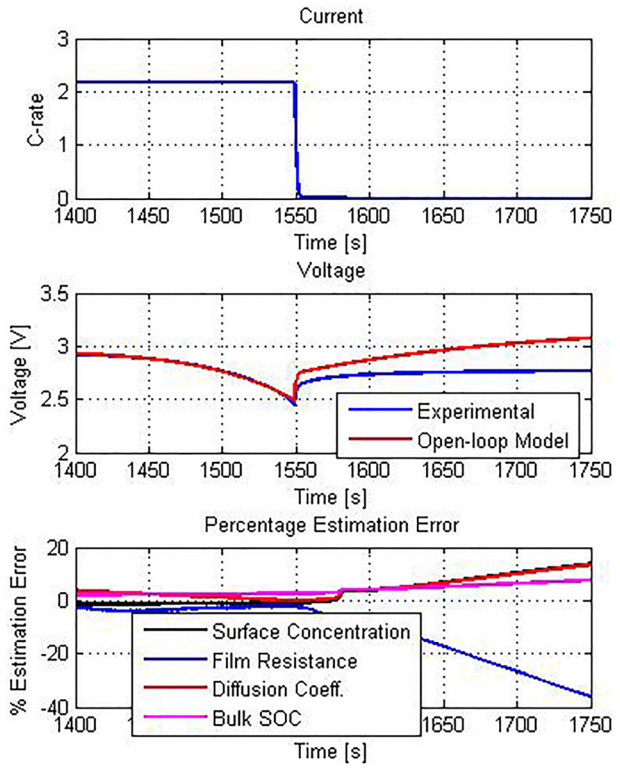

Fig. 13 Performance of the adaptive observer scheme in presence of output uncertainties and absence of input current

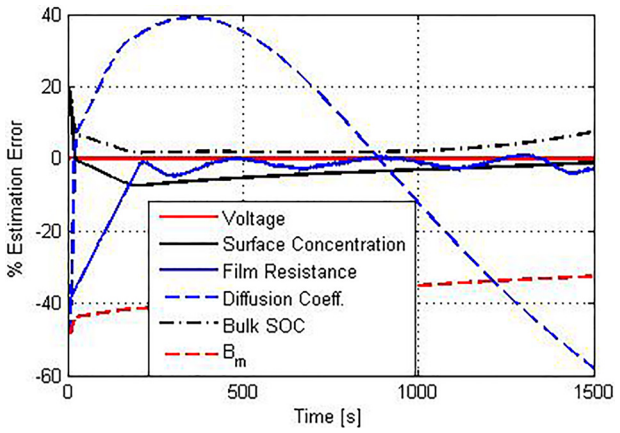

Fig. 14 Percentage errors in state and parameter estimation with high initial error in $\tilde{B}_M$

High Initial Error in B_M Estimation. During experimental and simulation studies, one observation we made is that the overall performance of the adaptive scheme degrades with high initial error $\tilde{B}_M$. In Fig. 13, one such scenario is illustrated under 2C constant discharge current. The variable $\hat{B}_M$ is initialized with 50% error. Note that the surface concentration, contact resistance, and voltage estimation computed via Observer I are reasonably good. However, the performance of Observer II degrades significantly as evident from the diverging errors in the Bulk SOC estimate and diffusion coefficient estimates. The probable reason for this degraded performance lies in the fact that the reduced model is only locally identifiable or observable. This limitation of the design can be easily overcome by minimizing the initial error in $\hat{B}_M$ with accurate accounting for the initial active material volume fraction of the specific battery cell.

Conclusion

In this paper, an adaptive observer design is presented for simultaneous state and parameter estimation of a Li-ion battery cell. It addresses the combined estimation of SOC and some electrochemical parameters, namely, diffusion coefficient, contact resistance, and active material volume fraction of the negative electrode, which are key requirements for advanced BMS. The proposed design considers the coupling between electrochemical and thermal dynamics of the cell. The design is split into two cascaded observers each of which is designed based on Lyapunov's stability analysis. A systematic approach is provided for the selection of the relevant gains of the design. Simulation and experimental studies are included which showed the effectiveness of the design in estimating the Li-ion concentration distribution, which gives both the bulk and surface SOC, and some electrochemical parameters, with a desired convergence rate and accuracy. Particularly, from the experimental studies it is found that the steady-state bulk SOC and surface concentration estimation errors lie within 5%. The parameter estimation steady-state error for contact resistance and diffusion coefficient lies within 15% and 5%, respectively. In case of B_M estimation error, the steady-state error is around 2%, however, at the cost of smaller initialization error.

However, there are some limitations of this adaptive observer scheme that need special attention in implementation and should be subject to further study. First, a high initial error in the input coefficient parameter estimate degrades the performance of the scheme. Second, the stability of the overall scheme is not guaranteed under persistently zero input current and in the presence of large output uncertainties. As another future extension of this work, the proposed observer's performance can be studied under different operating conditions such as higher C-rates and low temperature.

Acknowledgment

This research was supported, in part, by the U.S. Department of Energy GATE program under Grant No. DE-EE0005571 and NSF under Grant No. CMMI-1055254.

Nomenclature

A = current collector area (cm^2)
A_s = cell surface area exposed to surroundings (cm^2)
$a_s^{\pm}$ = specific surface area (cm^2/cm^3)
c_e = electrolyte phase Li-ion concentration (mol/cm^3)
C_p = specific heat capacity (J/g K)
$c_s^{\pm}$ = solid phase Li-ion concentration (mol/cm^3)
$c_{s,e}^{\pm}$ = solid-phase Li-ion surface-concentration (mol/cm^3)
$c_{s,max}^{\pm}$ = solid-phase Li-ion max. concentration (mol/cm^3)
$D_s^{\pm}$ = diffusion coefficient in solid-phase (cm^2/s)
$D_{s,ref}^{\pm}$ = diffusion coefficient at T_{ref} (cm^2/s)
$E_K^{\pm}$ = activation energy of diffusion coefficient (J/mol)
$E_{Ds}^{\pm}$ = activation energy of reaction rate constant (J/mol)
F = Faraday's constant (C/mol)
h = heat transfer coefficient of the cell (W/cm^2 K)
I = current (A)
$K^{\pm}$ = reaction rate constant ($cm^{2.5}/mol^{0.5}/s$)
$K_{ref}^{\pm}$ = reaction rate constant at T_{ref} ($cm^{2.5}/mol^{0.5}/s$)
$L^{\pm}$ = length of the cell (cm)
r = radial coordinate (cm)
R = radius of solid active particle (cm)
$\bar{R}$ = universal gas constant (J/mol K)
R_f = contact resistance (Ω)
R_{f0} = constant part of contact resistance (Ω)
T = temperature (K)
T_{ref} = reference temperature (K)
T_∞ = temperature of cooling fluid (K)
$U^{\pm}$ = open circuit potential (V)
α = proportional constant of contact resistance (Ω/K)
$\bar{\alpha}^{\pm}$ = charge transfer coefficient
v = cell volume (cm^3)
ρ = cell density (g/cm^3)

Superscript

$\pm$ = positive/negative electrode

References

[1] Hatzell, K. B., Sharma, A., and Fathy, H. K., 2012, "A Survey of Long-Term Health Modeling, Estimation, and Control of Lithium-Ion Batteries: Challenges and Opportunities," American Control Conference (ACC), Montreal, Canada, June 27–29, pp. 584–591.
[2] Saha, B., Goebel, K., Poll, S., and Christophersen, J., 2007, "An Integrated Approach to Battery Health Monitoring Using Bayesian Regression and State Estimation," IEEE Autotestcon Conference, Baltimore, MD, Sept. 17–20, pp. 646–653.
[3] Ng, K. S., Moo, C., Chen, Y., and Hsieh, Y., 2009, "Enhanced Coulomb Counting Method for Estimating State-of-Charge and State-of-Health of Lithium-Ion Batteries," Appl. Energy, **86**(9), pp. 1506–1511.
[4] Plett, G. L., 2004, "Extended Kalman Filtering for Battery Management Systems of LiPB-Based HEV Battery Packs: Part 3. State and Parameter Estimation," J. Power Sources, **134**(2), pp. 277–292.
[5] Remmlinger, J., Buchholz, M., Meiler, M., Bernreuter, P., and Dietmayer, K., 2011, "State-of-Health Monitoring of Lithium-Ion Batteries in Electric Vehicles by On-Board Internal Resistance Estimation," J. Power Sources, **196**(12), pp. 5357–5363.
[6] Kim, I.-S., 2010, "A Technique for Estimating the State of Health of Lithium Batteries Through a Dual-Sliding-Mode Observer," IEEE Trans. Power Electron., **25**(4), pp. 1013–1022.
[7] Gould, C. R., Bingham, C. M., Stone, D. A., and Bentley, P., 2009, "New Battery Model and State-of-Health Determination Through Subspace Parameter Estimation and State-Observer Techniques," IEEE Trans. Veh. Technol., **58**(8), pp. 3905–3916.
[8] Chaturvedi, N. A., Klein, R., Christensen, J., Ahmed, J., and Kojic, A., 2010, "Algorithms for Advanced Battery-Management Systems," IEEE Control Syst. Mag., **30**(3), pp. 49–68.
[9] Doyle, M., Fuller, T. F., and Newman, J., 1993, "Modeling of Galvanostatic Charge and Discharge of the Lithium/Polymer/Insertion Cell," J. Electrochem. Soc., **140**(6), pp. 1526–1533.
[10] Kehs, M. A., Beeney, M. D., and Fathy, H. K., 2014, "Computational Efficiency of Solving the DFN Battery Model Using Descriptor Form With Legendre Polynomials and Galerkin Projections," American Control Conference (ACC), Portland, OR, June 4–6, pp. 260–267.
[11] Smith, K. A., Rahn, C. D., and Wang, C., 2010, "Model-Based Electrochemical Estimation and Constraint Management for Pulse Operation of Lithium Ion Batteries," IEEE Trans. Control Syst. Technol., **18**(3), pp. 654–663.
[12] Klein, R., Chaturvedi, N. A., Christensen, J., Ahmed, J., Findeisen, R., and Kojic, A., 2013, "Electrochemical Model Based Observer Design for a Lithium-Ion Battery," IEEE Trans. Control Syst. Technol., **21**(2), pp. 289–301.
[13] Forman, J. C., Bashash, S., Stein, J. L., and Fathy, H. K., 2011, "Reduction of an Electrochemistry-Based Li-Ion Battery Model Via Quasi-Linearization and Pade Approximation," J. Electrochem. Soc., **158**(2), pp. A93–A101.
[14] Docimo, D. J., Ghanaatpishe, M., and Fathy, H. K., 2014, "Development and Experimental Parameterization of a Physics-Based Second-Order Lithium-Ion Battery Model," ASME Paper No. DSCC2014-6270.
[15] Santhanagopalan, S., and White, R. E., 2006, "Online Estimation of the State of Charge of a Lithium Ion Cell," J. Power Sources, **161**(2), pp. 1346–1355.
[16] Domenico, D., Stefanopoulou, A., and Fiengo, G., 2010, "Lithium-Ion Battery State of Charge and Critical Surface Charge Estimation Using an Electrochemical Model-Based Extended Kalman Filter," ASME J. Dyn. Syst., Meas., Control, **132**(6), p. 061302.
[17] Moura, S. J., Chaturvedi, N. A., and Krstic, M., 2012, "PDE Estimation Techniques for Advanced Battery Management Systems—Part I: SOC Estimation," American Control Conference (ACC), pp. 559–565.
[18] Dey, S., and Ayalew, B., 2014, "Nonlinear Observer Designs for State-of-Charge Estimation of Lithium-Ion Batteries," American Control Conference (ACC), Portland, OR, June 4–6, pp. 248–253.
[19] Dey, S., Ayalew, B., and Pisu, P., "Nonlinear Robust Observers for State-of-Charge Estimation of Lithium-Ion Cells Based on a Reduced Electrochemical Model," IEEE Trans. Control Syst. Technol. (online).
[20] Samadi, M. F., Alavi, S. M., and Saif, M., 2013, "Online State and Parameter Estimation of the Li-Ion Battery in a Bayesian Framework," American Control Conference (ACC), Washington, DC, June 17–19, pp. 4693–4698.
[21] Schmidt, A. P., Bitzer, M., Imre, Á. W., and Guzzella, L., 2010, "Model-Based Distinction and Quantification of Capacity Loss and Rate Capability Fade in Li-Ion Batteries," J. Power Sources, **195**(22), pp. 7634–7638.
[22] Fang, H., Wang, Y., Sahinoglu, Z., Wada, T., and Hara, S., 2013, "Adaptive Estimation of State of Charge for Lithium-Ion Batteries," American Control Conference (ACC), pp. 3485–3491.
[23] Fang, H., Wang, Y., Sahinoglu, Z., Wada, T., and Hara, S., 2014, "State of Charge Estimation for Lithium-Ion Batteries: An Adaptive Approach," Control Eng. Pract., **25**, pp. 45–54.

[24] Moura, S. J., Chaturvedi, N. A., and Krstic, M., 2013, "Adaptive PDE Observer for Battery SOC/SOH Estimation Via an Electrochemical Model," ASME J. Dyn. Syst., Meas., Control, **136**(1), p. 011015.
[25] Wang, Y., Fang, H., Sahinoglu, Z., Wada, T., and Hara, S., 2013, "Nonlinear Adaptive Estimation of the State of Charge for Lithium-Ion Batteries," 52nd Annual Conference on Decision and Control, pp. 4405–4410.
[26] Wang, Y., Fang, H., Sahinoglu, Z., Wada, T., and Hara, S., 2015, "Adaptive Estimation of the State of Charge for Lithium-Ion Batteries: Nonlinear Geometric Observer Approach," IEEE Trans. Control Syst. Technol., **23**(3), pp. 948–962.
[27] Dey, S., Ayalew, B., and Pisu, P., 2014, "Combined Estimation of State-of-Charge and State-of-Health of Li-Ion Battery Cells Using SMO on Electrochemical Model," 13th International Workshop on Variable Structure Systems, Nantes, France, June 29–July 2, pp. 1–6.
[28] Zhou, X., Ersal, T., Stein, J. L., and Bernstein, D. S., 2013, "Battery Health Diagnostics Using Retrospective-Cost Subsystem Identification: Sensitivity to Noise and Initialization Errors," ASME Paper No. DSCC2013-3953.
[29] Zhou, X., Ersal, T., Stein, J. L., and Bernstein, D. S., 2014, "Battery State of Health Monitoring by Side Reaction Current Density Estimation Via Retrospective-Cost Subsystem Identification," ASME Paper No. DSCC2014-6254.
[30] Debert, M., Colin, G., Bloch, G., and Chamaillard, Y., 2013, "An Observer Looks at the Cell Temperature in Automotive Battery Packs," Control Eng. Pract., **21**(8), pp. 1035–1042.
[31] Lin, X., Perez, H. E., Mohan, S., Siegel, J. B., Stefanopoulou, A. G., Ding, Y., and Castanier, M. P., 2014, "A Lumped-Parameter Electro-Thermal Model for Cylindrical Batteries," J. Power Sources, **257**, pp. 1–11.
[32] Lin, X., Perez, H. E., Siegel, J. B., Stefanopoulou, A. G., Li, Y., Anderson, R. D., Ding, Y., and Castanier, M. P., 2013, "Online Parameterization of Lumped Thermal Dynamics in Cylindrical Lithium Ion Batteries for Core Temperature Estimation and Health Monitoring," IEEE Trans. Control Syst. Technol., **21**(5), pp. 1745–1755.
[33] Kim, Y., Mohan, S., Siegel, J. B., Stefanopoulou, A. G., and Ding, Y., 2014, "The Estimation of Temperature Distribution in Cylindrical Battery Cells Under Unknown Cooling Conditions," IEEE Trans. Control Syst. Technol., **22**(6), pp. 2277–2286.
[34] Lin, X., Fu, H., Perez, H. E., Siegel, J. B., Stefanopoulou, A. G., Ding, Y., and Castanier, M. P., 2013, "Parameterization and Observability Analysis of Scalable Battery Clusters for Onboard Thermal Management," Oil Gas Sci. Technol., **68**(1), pp. 165–178.
[35] Tanim, T. R., Rahn, C. D., Wang, C.-Y., 2015, "State of Charge Estimation of a Lithium Ion Cell Based on a Temperature Dependent and Electrolyte Enhanced Single Particle Model," Energy, **80**(1), pp. 731–739.
[36] Klein, R., Chaturvedi, N. A., Christensen, J., Ahmed, J., Findeisen, R., and Kojic, A., 2010, "State Estimation of a Reduced Electrochemical Model of a Lithium-Ion Battery," American Control Conference (ACC), Baltimore, MD, June 30–July 2, pp. 6618–6623.
[37] Bandhauer, T. M., Garimella, S., and Fuller, T. F., 2011, "A Critical Review of Thermal Issues in Lithium-Ion Batteries," J. Electrochem. Soc., **158**(3), pp. R1–R25.
[38] Dey, S., Ayalew, B., and Pisu, P., 2014, "Adaptive Observer Design for a Li-Ion Cell Based on Coupled Electrochemical-Thermal Model," ASME Paper No. DSCC2014-5986.
[39] Guo, M., Sikha, G., and White, R. E., 2011, "Single-Particle Model for a Lithium-Ion Cell: Thermal Behavior," J. Electrochem. Soc., **158**(2), pp. A122–A132.
[40] Ramadass, P., Haran, B., White, R., and Popov, B. N., 2003, "Mathematical Modeling of the Capacity Fade of Li-Ion Cells," J. Power Sources, **123**(2), pp. 230–240.
[41] Smith, K., and Wang, C. Y., 2006, "Power and Thermal Characterization of a Lithium-Ion Battery Pack for Hybrid-Electric Vehicles," J. Power Sources, **160**(1), pp. 662–673.
[42] Rahimian, S. K., Rayman, S., and White, R. E., 2013, "Extension of Physics-Based Single Particle Model for Higher Charge–Discharge Rates," J. Power Sources, **224**, pp. 180–194.
[43] Luo, W., Lyu, C., Wang, L., and Zhang, L., 2013, "A New Extension of Physics-Based Single Particle Model for Higher Charge–Discharge Rates," J. Power Sources, **241**, pp. 295–310.
[44] Tanim, T. R., Rahn, C. D., and Wang, C. Y., 2014, "A Temperature Dependent, Single Particle, Lithium Ion Cell Model Including Electrolyte Diffusion," ASME J. Dyn. Syst., Meas., Control, **137**(1), p. 011005.
[45] Vetter, J., Novák, P., Wagner, M. R., Veit, C., Möller, K.-C., Besenhard, J. O., Winter, M., Wohlfahrt-Mehrens, M., Vogler, C., and Hammouche, A., 2005, "Ageing Mechanisms in Lithium-Ion Batteries," J. Power Sources, **147**(1–2), pp. 269–281.
[46] Cho, Y. M., and Rajamani, R., 1997, "A Systematic Approach to Adaptive Observer Synthesis for Nonlinear Systems," IEEE Trans. Autom. Control, **42**(4), pp. 534–537.
[47] Rajamani, R., and Hedrick, J. K., 1995, "Adaptive Observers for Active Automotive Suspensions: Theory and Experiment," IEEE Trans. Control Syst. Technol., **3**(1), pp. 86–93.
[48] Slotine, J. J. E., and Li, W., 1991, *Applied Nonlinear Control*, Prentice-Hall, Upper Saddle River, NJ.
[49] Narendra, K. S., and Annaswamy, A., 1989, *Stable Adaptive Systems*, Prentice-Hall, Englewood Cliffs, NJ.
[50] Prada, E., Domenico, D., Creff, Y., Bernard, J., Sauvant-Moynot, V., and Huet, F., 2012, "Simplified Electrochemical and Thermal Model of $LiFePO_4$–Graphite Li-Ion Batteries for Fast Charge Applications," J. Electrochem. Soc., **159**(9), pp. A1508–A1519.
[51] Arora, P., Doyle, M., Gozdz, A. S., White, R. E., and Newman, J., 2000, "Comparison Between Computer Simulations and Experimental Data for High-Rate Discharges of Plastic Lithium-Ion Batteries," J. Power Sources, **88**(2), pp. 219–231.
[52] Delacourt, C., and Safari, M., 2011, "Analysis of Lithium Deinsertion/Insertion in LiyFePO4 With a Simple Mathematical Model," Electrochim. Acta, **56**(14), pp. 5222–5229.
[53] Santhanagopalan, S., Guo, Q., Ramadass, P., and White, R. E., 2006, "Review of Models for Predicting the Cycling Performance of Lithium Ion Batteries," J. Power Sources, **156**(2), pp. 620–628.
[54] Siegel, J. B., Lin, X., Stefanopoulou, A. G., Hussey, D. S., Jacobson, D. L., and Gorsich, D., 2011, "Neutron Imaging of Lithium Concentration in LFP Pouch Cell Battery," J. Electrochem. Soc., **158**(5), pp. A523–A529.